The global overturning circulation and the importance of non-equilibrium effects in ECCOv4r3

Tatsu Monkman[1] and Malte Friedrich Jansen[2]

[1]The University of Chicago
[2]University of Chicago

November 22, 2022

Abstract

We quantify the volume transport and watermass transformation rates of the global ocean circulation using data from the Estimating the Circulation and Climate of the Ocean version 4 release 3 (ECCOv4r3) reanalysis product. Our results support large rates of intercell exchange between the mid-depth and abyssal cells, in agreement with modern theory and observations. However, the present-day circulation in ECCO cannot be interpreted as a near-equilibrium solution. Instead, a dominant portion of the apparent diapycnal transport of watermasses within the deep ocean is associated with isopycnal volume change, rather than diabatic processes, reflecting trends in the deep ocean density structure. Our results imply two possibilities: either such trends in ECCOv4r3 are unrealistic, implying that ECCO's representation of the overturning circulation and watermass transformations are inconsistent, or the trends in ECCOv4r3 are realistic and equilibrium theories of the overturning circulation cannot be applied to the present-day ocean.

The global overturning circulation and the importance of non-equilibrium effects in ECCOv4r3

Tatsu Monkman[1] **and Malte F. Jansen**[1]

[1]The University of Chicago

Key Points:

- The MOC in ECCOv4r3 exhibits substantial linkage between the mid-depth and abyssal cells.
- Transient isopycnal volume change is prevalent in ECCO's deep ocean and heavily influences the MOC.
- ECCO's transient interior state must be taken into account when studying its climatological state.

Corresponding author: Tatsu Monkman, `tdmonkman@uchicago.edu`

Abstract

We quantify the volume transport and watermass transformation rates of the global ocean circulation using data from the Estimating the Circulation and Climate of the Ocean version 4 release 3 (ECCOv4r3) reanalysis product. Our results support large rates of intercell exchange between the mid-depth and abyssal cells, in agreement with modern theory and observations. However, the present-day circulation in ECCO cannot be interpreted as a near-equilibrium solution. Instead, a dominant portion of the apparent diapycnal transport of watermasses within the deep ocean is associated with isopycnal volume change, rather than diabatic processes, reflecting trends in the deep ocean density structure. Our results imply two possibilities: either such trends in ECCOv4r3 are unrealistic, implying that ECCO's representation of the overturning circulation and watermass transformations are inconsistent, or the trends in ECCOv4r3 are realistic and equilibrium theories of the overturning circulation cannot be applied to the present-day ocean.

Plain Language Summary

We analyze data taken from the Estimating the Circulation and Climate of the Ocean (ECCOv4r3) data product in order to investigate the internal structure and drivers of the global ocean's large-scale circulation. The ECCO product is a physically consistent estimate of the global ocean's state generated by fitting a computational ocean model to a suite of oceanographic observations. Our results support the modern view of an interconnected global ocean with substantial exchange between the overturning circulation of the Atlantic and that of the Indo-Pacific via the Southern Ocean. However, our investigation also reveals that much of the deep ocean in the ECCO product is in a state of change and these changes play a key role in the circulation. These results call into question either the model's representation of the deep ocean or the prevailing theoretical depictions of the ocean's large-scale circulation, which generally assume that the ocean is in a steady state.

1 Introduction

The global meridional overturning circulation (MOC) modulates the exchange of watermasses between the surface and the deep ocean, between different latitudes and between the Atlantic and Indo-Pacific Oceans via the Southern Ocean, and facilitates a large portion of the world's heat transport and carbon dioxide uptake (Toggweiler et al., 2006; Ferrari & Ferreira, 2011). The global MOC is often described in terms of two circulation cells: the mid-depth cell and the abyssal cell. The mid-depth cell is primarily located in the upper- and mid-depths of the Atlantic Ocean and is associated with the formation of North Atlantic Deep Water (NADW) via surface transformations in the north and wind-driven upwelling in the south (Marshall & Speer, 2012). The abyssal cell, which occupies much of the deep and abyssal Indo-Pacific basin, is associated with Antarctic Bottom Water (AABW) formation off the coast of Antarctica (Gordon, 2001)) and diffusive upwelling in the ocean interior (Weaver et al., 1999). Both cells play a major role in Earth's climate: the mid-depth cell contributes to poleward heat transport in the Northern Hemisphere (Wunsch, 2005), while the abyssal cell subsumes CO2 and heat anomalies into the ocean interior (Sarmiento, 2019; Russel et al., 2006; Marshall & Speer, 2012; Adkins, 2013). Changes in either limb of the MOC could have a profound effect on both regional and global-scale climate (e.g. Zhang et al. (2019)).

Despite the importance of the MOC to Earth's past and future climate, our understanding of the MOC's interior structure is incomplete. Crucially, we still lack a clear consensus on the exchange rate of volume between the mid-depth and abyssal cells, and on the role and rates of diapycnal diffusion, which governs the interior watermass transformations thought to be critical to maintaining the MOC. Our incomplete understanding of the structure of the deep ocean circulation and the water mass transformations that govern it leads to uncertainty in predicting its role in future and past climate shifts, and serves as motivation for this study.

Our first objective is to study the return pathways of NADW and the amount of inter-cell coupling within the MOC in ECCOv4r3. Observational and theoretical evidence supports a large amount of exchange between the mid-depth and abyssal cells via the Southern Ocean, although there is some disagreement about the actual magnitude of exchange that occurs. Hydrographic analysis by Talley (2013) suggests that most NADW is converted to abyssal-cell AABW near the coast of Antarctica ($\sim$13Sv), and re-circulates through the abyssal cell before returning into the Atlantic (c.f. Ferrari et al. (2014)). Inverse analysis by Lumpkin and Speer (2007) meanwhile shows a more even partitioning of NADW between the abyssal cell ($\sim$11Sv) and recirculation within the mid-depth cell ($\sim$7Sv), and a roughly similar partitioning is found by Cessi (2019) in the ECCOv4r2 state estimate (spanning 1992-2011). A recent study by Rousselet et al. (2021) uses Lagrangian drifters in ECCOv4r3 to find a similar partition of NADW between "upper" (32%) and "lower" (78%) recirculation routes, and argues that the lower route is further partitioned into an abyssal route through the Indo-Pacific (48%) and a "subpolar" cell route (20%) localized to the Southern Ocean. Here, we seek to quantify the fate of NADW from a basin-wide net isopycnal volume budget perspective in ECCOv4r3, thus focusing on the overall strengths of the various circulation limbs, rather than the pathways taken by individual water parcels (as addressed by Rousselet et. al., 2021). In our study, inter-cell exchange is defined based on the amount of NADW that leaves the Atlantic below the isopycnal that separates the mid-depth and abyssal cells in the Southern Ocean. This volume transport must, by volume conservation, be balanced by a similar amount of net upwelling in the Indo-Pacific.

Our second objective is to investigate the interior watermass transformations that maintain the MOC. Theoretical models of the MOC capture its large-scale dynamics generally under the assumption that the present-day ocean is in an equilibrium state (Nikurashin & Vallis, 2011; Wolfe & Cessi, 2011; Thompson et al., 2016). Studies such as Gnanadesikan (1999) and Wolfe and Cessi (2011) show that single-basin models with a southern re-entrant channel, where deep water formation in the north is balanced by wind-driven upwelling in the south, can recreate an adiabatic circulation that captures the magnitude and major characteristics of the mid-depth cell (Lumpkin & Speer, 2007) - such an "adiabatic" mid-depth cell does note require any interior watermass transformations. The abyssal cell, meanwhile, is thought to be fundamentally governed by diabatic processes in the ocean interior, with negative surface buoyancy fluxes near the southern boundary balancing diffusive density loss and upwelling in the basin interiors to the north (Nikurashin & Vallis, 2011). In both cases the models hinge on the assumption that diapycnal transport is balanced exactly by irreversible watermass transformations, either via surface fluxes of heat and freshwater or via diapycnal mixing in the interior, giving a steady-state ocean circulation. We seek to investigate the degree to which ECCOv4r3's MOC adheres to such circulation regimes and whether the common equilibrium assumption is valid when applied to the present-day ocean.

Our results support the general view of an interconnected global overturning circulation, as described in previous studies (e.g. Ferrari et al. (2017); Talley (2013); Cessi (2019)). However, our results also reveal that ECCOv4r3's deep ocean is not in equilibrium and that isopycnal volume changes, associated with trends in the deep ocean density, play a key role in the interior circulation pathways.

2 Data and Methods

2.1 Dataset: ECCOv4r3

We analyze data from the ECCOv4r3 ocean state estimate (Forget et al., 2015; ECCO Consortium et al., 2017; Fukumori et al., 2017). The ECCOv4 setup comprises a non-linear inverse modelling framework utilizing the MITgcm ocean model (Marshall et al., 1997) in conjunction with the adjoint method (Forget & Ponte, 2015) to produce an optimized baseline solution of the hydrostatic Boussinesq equations, fit to a suite of oceanographic data spanning the time period of 1992-2015 (Forget et al., 2015). The MITgcm comprises the model component of ECCOv4r3 and is computed on the LLC90 grid with a latitudinally-varying horizontal resolution between approximately 20km-40km at 80^oN/S to 110km at 10^oN/S. Further details about the ECCO state estimate are provided in Forget et al. (2015).

2.2 The Meridional Overturning Circulation in Potential Density Coordinates

We compute the isopycnal meridional overturning streamfunction, ψ, to evaluate the overall volume budgets of the global ocean circulation, subdivided by ocean basin. We perform our calculations in potential density space referenced to 2000dbar (henceforth σ), the approximate average local pressure of NADW within the Atlantic interior, which is consistent with Cessi (2019) and Rousselet et al. (2021). We compute the height of each isopycnal layer by linearly interpolating σ values between depth levels, and compute transports by assuming vertically constant velocities within each grid box. The time-mean of ψ as a function of potential density (σ) and latitude (y), $\psi(\sigma, y)$, is derived from the ECCOv4r3 diagnostic fields by vertically integrating the sum of the resolved meridional transport, $\mathbf{v}(x, y, z, t)$, and the GM-parameterized meridional eddy transport, $\mathbf{v}^*(x, y, z, t)$, from the ocean bottom to a given σ surface and then integrating zonally and averaging in time:

$$\psi(\sigma, y) = \overline{\int_{x_0(y)}^{x_1(y)} \int_{-H(x,y)}^{z(\sigma,x,y,t)} \mathbf{v}(x, y, z, t) + \mathbf{v}^*(x, y, z, t) dz dx}, \tag{1}$$

where x denotes longitude and $\int_{x_0(y)}^{x_1(y)} dx$ gives the zonal integral at a given latitude y across an ocean basin bounded by longitudes x_0 and x_1. The overline denotes the time-average of the enclosed quantity over the full ECCO time period. $H(x, y)$ denotes the ocean depth and $z(\sigma, x, y, t)$ gives the depth of an isopycnal surface σ at a particular location. We calculate ψ by integrating across the Atlantic, Southern, and Indo-Pacific ocean basins, which in turn are divided by the continents and the 32^oS parallel (Figure S1).

2.3 Volume Budget Decomposition in the Interior

We employ an isopycnal volume-budget analysis based on Walin (1982) to diagnose the processes that balance diapycnal advection within the large-scale circulation in ECCOv4r3. We consider a volume flux balance across the surface of an isopycnal volume of ocean, $V(\sigma, y_1, y_2)$, bounded above by an isopycnal of density σ, in the zonal direction by continental boundaries, and in the south, y_1, and north, y_2, by either a latitudinal basin boundary or the latitude where the isopycnal outcrops into the surface layer. We define the bottom of the surface layer as the maximum surface potential density at or equatorwards of any given latitude over the entire ECCO period (i.e., the bottom of the surface layer as defined here is not itself a function of time). Following volume conservation, the total volume budget for an interior isopycnal volume can be expressed as:

$$\Delta\psi = \overline{\frac{d}{dt} V(\sigma, y_1, y_2, t)} + \overline{T_{geo}(\sigma, y_1, y_2, t)} + \overline{T_{mix}(\sigma, y_1, y_2, t)}. \tag{2}$$

Here $\Delta\psi = \psi(\sigma, y_2) - \psi(\sigma, y_1)$ is the net transport across the northern and southern boundaries. $\overline{\frac{d}{dt} V(\sigma, y_1, y_2, t)}$ is the time-averaged change in the total volume itself (Newsom et al., 2016; de Lavergne et al., 2016):

$$\frac{d}{dt}V(\sigma, y_1, y_2, t) = \frac{d}{dt}\iint_{A_\sigma(y_1,y_2)} h(\sigma, x, y, t)dA, \tag{3}$$

where $h(\sigma, x, y, t)$ is the height of the isopycnal above the ocean bottom and $A_\sigma(y_1, y_2)$ is the isopycnal area bounded in the south and north by y_1 and y_2, respectively. $T_{geo}(\sigma, y_1, y_2, t)$ is the diapycnal transport due to geothermal heating:

$$T_{geo}(\sigma, y_1, y_2, t) = -\frac{\partial}{\partial\sigma}\iint_{A_I(\sigma,y_1,y_2,t)} \frac{\alpha Q_{geo}(x, y)}{c_p}dA, \tag{4}$$

where $A_I(\sigma, y_1, y_2, t)$ is the area where the bottom density $\sigma_b \geq \sigma$ within the domain bounded by y_1, y_2, and the sides of the basin, $Q_{geo}(x, y)$ is the geothermal heat flux at the ocean floor, $\alpha = -\frac{1}{\sigma}\frac{\partial\sigma}{\partial\theta}$ is the thermal expansion coefficient, and c_p is the heat capacity of seawater (see de Lavergne et al. (2016) for a full derivation). $T_{mix}(\sigma, y_1, y_2, t)$ represents the watermass transformation rate due to mixing processes, which we compute as a residual of the other terms due to the difficulty in accounting for numerical diapycnal mixing, parameterized mixing due to the Gaspar, Gregoris, and Lefevre (GGL) scheme (Gaspar et al., 1990), and horizontal mixing in the presence of slope-clipping along steep isopycnals. By applying (2) to specific domains of interest, we can estimate the major drivers of interior water mass transformations occurring within them. A schematic of our volume budget decomposition applied to the Atlantic, Indo-Pacific, and Southern Ocean basins is included in the supplement (Figure S2). For completeness, we also perform a similar volume budget decomposition for the surface layers in the Southern Ocean and North Atlantic, which is detailed in the SI.

3 Results

The isopycnal overturning in ECCOv4r3 (Figure 1) is qualitatively similar to that derived in other studies (e.g. Lumpkin and Speer (2007)) and the magnitudes of the overturning cells generally fall within uncertainties established by observational estimates, as previously found for ECCOv4r2 by Cessi (2019). The mid-depth cell occupies the Atlantic with a peak overturning strength of 18.7Sv occurring at 55^{o}N, in good agreement with other observational estimates (Lumpkin & Speer, 2007; Talley, 2013). The abyssal cell dominates the Indo-Pacific and the lower part of the Southern Ocean and peaks at approximately 14.1Sv at 36^{o}S, a substantially weaker value than that derived by Lumpkin and Speer (2007) (20Sv), Talley (2013) (29Sv), and Kunze (2017) (20Sv), but similar to the estimates of de Lavergne et al. (2016) (10-15Sv). The abyssal cell in our analysis is also weaker than the value reported in Cessi (2019) (20Sv, at 30S), who employed ECCO version 4 release 2.

Large-scale diapycnal transport is visible in the Atlantic and Indo-Pacific Oceans. In the Atlantic $\sim$4.2Sv of NADW upwell diabatically across the σ=1036.8kg/m^3 isopycnal and return to the surface in the North Atlantic (Figure 1a). Moreover, we see persistent downwelling across density surfaces in the lower range of NADW, yielding around 7.6Sv of transport across σ=1036.96kg/m^3 over the length of the Atlantic. The abyssal cell is almost entirely confined to the Indo-Pacific, where upwelling peaks at 14.1Sv at $\sigma = 1037.053$kg/m^3.

The net exchange of watermasses between the Atlantic's mid-depth cell and the abyssal cell can be found by considering the Atlantic, Indo-Pacific and Southern Ocean overturning stream functions at 32^{o}S. In ECCOv4r3, 14.5Sv of NADW exit the Atlantic at 32^{o}S, of which 5.3Sv enter the Southern Ocean at density classes occupied by the mid-depth cell ($\sigma < 1036.96$kg/m^3). The lower 9.2Sv of NADW enter the Southern Ocean in the density range of the abyssal cell ($\sigma \geq 1036.96$kg/m^3), and hence must be balanced by a similar amount of upwelling in the Indo-Pacific. Note that this analysis does

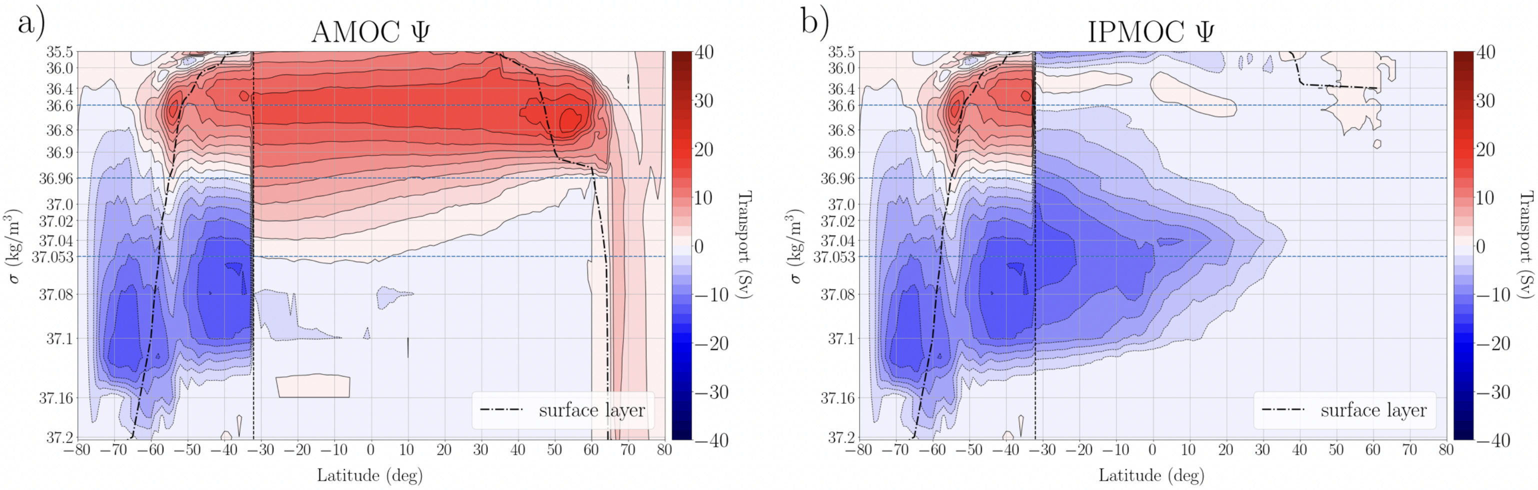

Figure 1. Atlantic, Indo-Pacific, and Southern Ocean stream functions in potential density space (referenced to 2000dbar), calculated from ECCOv4r3 and averaged over the full ECCO time period (1992-2015). (a) the Atlantic Meridional Overturning Circulation (AMOC) and (b) IndoPacific Meridional Overturning Circulation (IPMOC). The Southern Ocean Meridional Overturning Circulation is plotted in both (a) and (b) south of 32^{o}S. Positive (red) denotes clockwise flow and negative (blue) denotes counterclockwise flow (CL=2Sv). The dash-dotted line indicates the bottom of the surface layer. The vertical dashed line indicates the northern end of the Southern Ocean at 32^{o}S. Horizontal dashed lines denote specific density surfaces of interest: the upper bound of southward-flowing NADW: σ=1036.4kg/m^3, the division between the upper and lower cells in the Southern Ocean: σ=1036.96kg/m^3, and the maximum density of NADW entering the SO: σ=1037.05kg/m^3. The density-axis is stretched to reflect the average isopycnal depth within the Atlantic for σ<1037.1kg/m^3 (the maximum density in the Atlantic) and is extended linearly to the highest densities in the Southern Ocean. The same density axis is used in subsequent plots.

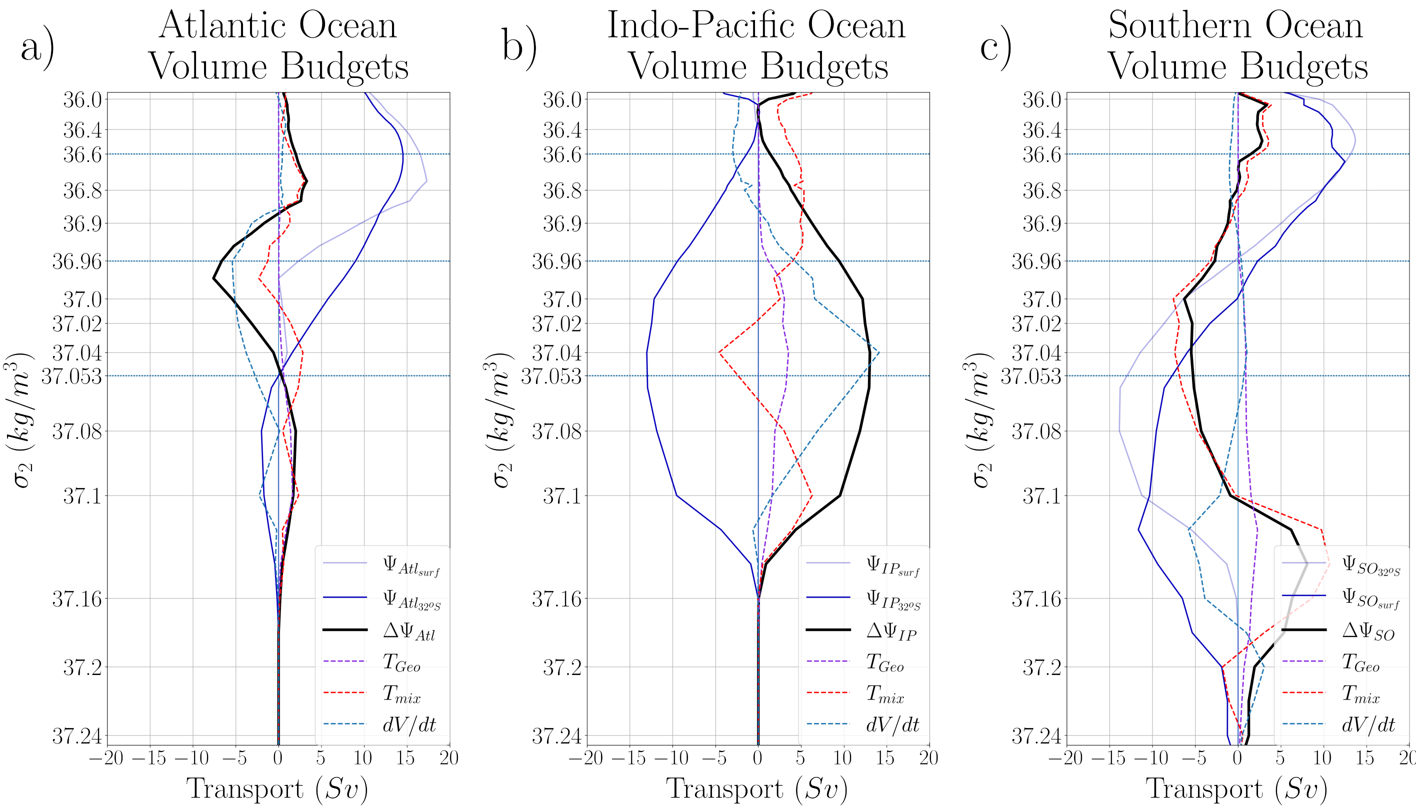

Figure 2. Volume budget decompositions across the Atlantic Ocean (**a**), IndoPacific Ocean (**b**), and Southern Ocean (**c**). Solid black lines denote net diapycnal transformation across density surfaces, inferred from the difference between Ψ^{σ} across each region's northern (light shading) and southern (dark shading) boundaries. The subscript $Surf$ refers to the stream function at the bottom of the surface layer, defined by the minimum surface density at a given latitude (Figure 1). The net diapycnal transport (solid black) is de-composed into contributions from: geothermal transformations (dashed purple), turbulent diffusive transformations (dashed red), and isopycnal volume change (dashed cyan).

not necessarily illuminate the pathways of individual water parcels, as we are only considering the net up- and downwelling across individual basins rather than actual particle trajectories, such as Rousselet (2021). Irrespective of the specific advective pathways, however, the density overlap between the two overturning cells is likely to lead to significantly enhanced inter-cell exchange (Nadeau et al., 2019).

The natural question that arises next is how the diapycnal up- and down-welling in the interior of the Atlantic and Indo-Pacific basins is balanced by watermass transformations, which will be discussed in the following section.

3.1 Volume Budget Analysis

We consider the isopycnal volume budgets in the Atlantic, Indo-Pacific, and Southern Ocean interiors (Figure 2). In the Atlantic, interior mixing-driven transformations peak at around ∼3.6Sv at $\sigma = 1036.8$, accounting for most of the observed diapycnal upwelling in the North Atlantic. Surprisingly, the majority of the apparent diapycnal downwelling of lower NADW in the Atlantic is associated with the volume tendency term, dV/dt, the contribution of which is higher than that of diapycnal mixing. The Atlantic volume tendency peaks at $\sigma = 1036.96\text{kg/m}^3$ with a value of -5.5Sv. Isopycnal surfaces in the deep Atlantic hence exhibit a steady downward movement over the course of the ECCOv4r3 time-span (1992-2015), which, when combined with a relatively small mixing-driven downward transport ($T_{mix} \approx$-2Sv), accounts for the time-mean downward transport of $\approx$7.6Sv at σ=1036.96. Cross isopycnal upwelling due to geothermal heat flux (T_{geo}) is significant only for the densest watermasses below σ=1037.053. The dense water formation in the north is associated primarily with surface heat loss within the North Atlantic region as well as dense water inflow across the Greenland-Iceland-Scotland (GIS) ridge system, with a smaller counteracting contribution from mixing within the surface layer (Figure S3).

Upwelling in the Indo-Pacific is also primarily associated with isopycnal volume change. dV/dt dominates the volume budget of the Indo-Pacific over much of the abyssal ocean, peaking at $\sigma = 1037.04\text{kg/m}^3$ with a value of 14.11Sv, which amounts to a significant shoaling of isopycnals over the ECCO timespan. The sign of the mixing-driven watermass transformation varies with depth, exhibiting two notable peaks with a maximum downward transfer of -5.0Sv at $\sigma = 1037.04\text{kg/m}^3$ and a maximum upward transfer of 6.2Sv at $\sigma = 1037.1\text{kg/m}^3$. Watermass transformations due to geothermal heating peaks at $\sigma = 1037.04\text{kg/m}^3$ with a value of 3.52Sv.

Both mixing and volume tendency terms are significant in the Southern Ocean. Mixing-driven downwelling is dominant between $\sigma = 1036.8\text{kg/m}^3$ and $\sigma = 1037.1\text{kg/m}^3$, which stands in contrast to the relatively low mixing-driven downwelling rates in the northern basins. Substantial mixing-driven upwelling is seen between $\sigma \approx\sim 1037.1\text{kg/m}^3$ and $\sigma =\approx 1037.2\text{kg/m}^3$, with a peak of 13.8Sv at $\sigma =\approx 1037.14\text{kg/m}^3$. This mixing-driven watermass transformation is partially compensated by a downward movement of density surfaces, leaving a net upwelling of 8Sv. Mixing also plays a major role in balancing the volume budgets within the surface layer in the Southern Ocean (Figure S3), consistent with previous results for course-resolution ocean models (Newsom et al., 2016).

4 Summary and Discussion

Our results support an interconnected view of the MOC (summarized in Figure 3), with substantial linkages between the AMOC and the abyssal cell. Although our analysis cannot isolate trajectories of individual water parcels, it is clear that substantial diapycnal upwelling in the Indo-Pacific is needed to balance the inflow of dense NADW into the Southern Ocean. We also find significant diapycnal up- and down-welling within the Atlantic, the latter of which is not typically included in idealized depictions of the mid-depth cell. In both ocean basins, much of the net diapycnal up- and down-welling is balanced by isopycnal volume changes, rather than mixing-driven watermass transformations as theoretical models usually assume.

The isopycnal depth trends in ECCOv4r3 represent vertical isopycnal displacement velocities on the order of +/- 5-20 m/yr and persist over the entire ECCOv4r3 time span (Figure 4 a,b). These trends are present in all of the major ocean basins and are relatively horizontally homogeneous over the Atlantic and Indo-Pacific basins (Figure 4, d,e). In the Atlantic, we see deepening isopycnals that correspond to an overall lightening of the deep ocean driven by warming temperatures and decreasing salinity. The deep Atlantic warming trend is broadly consistent with previous studies such as Palmer et al. (2015), Desbruyères et al. (2017), and Zanna et al. (2019), although these studies rely on many of the same data sources as ECCOv4r3 and are accompanied by large uncertainties. An under-representation of dense water inflows across the GIS ridges in ECCOv4r3 could also play a role in biasing deep Atlantic density trends by limiting the amount of dense water entering the Atlantic basin (Figure S3; Rossby et al. (2018); Lumpkin and Speer (2007); Lee et al. (2019); Tesdal and Haine (2020)), which may be compensated

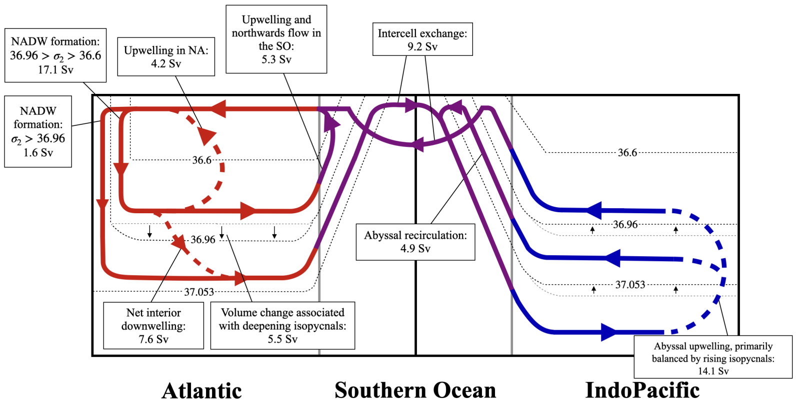

Figure 3. Schematic representation of the overturning, inferred from the stream function and volume budget decomposition (Figure 1, Figure 2). Net transport within the Atlantic Ocean (red arrows), Southern Ocean (purple arrows), and Indo-Pacific Ocean (blue arrows), are shown. Arrows denote direction of flow. Solid and dashed arrows below the surface denote primarily along- and across-isopycnal pathways, respectively. Dashed black lines denote the specific densities discussed in Figure 1, and isopycnal depth changes are indicated where they are the dominant contributor balancing up- and down-welling.

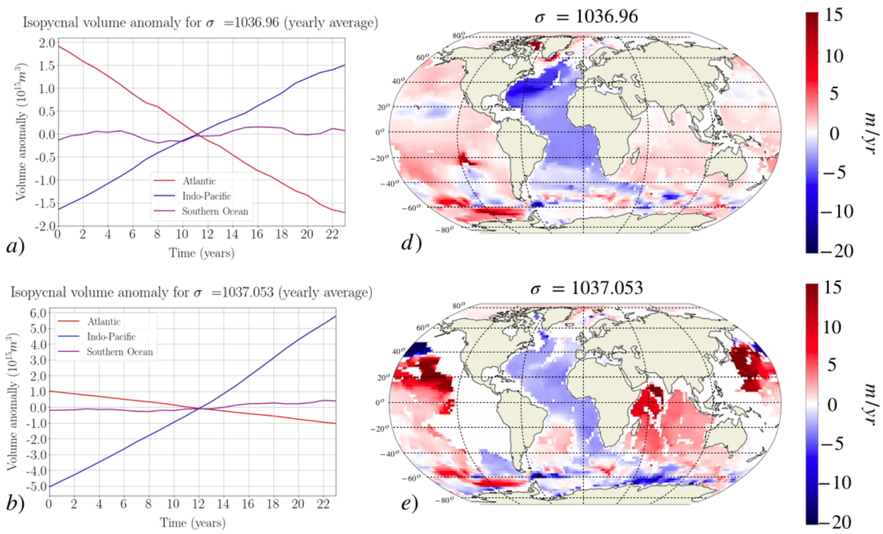

Figure 4. Trends in overall isopycnal volumes as calculated from yearly means and subdivided by basin (a, b), and spatial fields of time-averaged vertical isopycnal velocities, in meters per year, (d, e) for σ=1036.96kg/m^3 and σ=1037.053kg/m^3 over the ECCOv4r3 timespan (1992-2015). Striking linear trends are visible in the Atlantic and IndoPacific Oceans.

by spurious sinking of NADW during its southward path in ECCOv4r3. In the Indo-Pacific, meanwhile, we see isopycnal shoaling driven by a cooling of the abyssal ocean (c.f. Wunsch and Heimbach (2014); Liang et al. (2015)), which accounts for much of the abyssal cell upwelling in ECCOv4r3. Unfortunately, as argued by Wunsch and Heimbach (2014), it is impossible to infer whether these trends are the result of a) long-term trends in ocean climate, b) intrinsic ocean variability, or c) modeling and/or measurement/sampling biases.

Regardless of whether the simulated deep ocean density trends are real, we highlight their key role in the simulation and interpretation of the deep ocean overturning circulation and watermass transformations. The presence of isopycnal volume trends is especially important when interpreting ECCO's climatological mean state, as the implicit assumption of a stationary state (as e.g. in Rousselet et al. (2021)) leads to apparent interior watermass transformations that are actually associated with adiabatic trends in isopycnal depth.

The transient evolution of ECCOv4r3's deep ocean must also be taken into account when comparing the circulation to theoretical models that are based on an equilibrium assumption. In the equilibrium view of the global overturning circulation, deep water formation in the high latitudes must be balanced by wind-driven upwelling along isopycnals or irreversible processes in the ocean interior, which in turn are typically assumed to be dominated by diapycnal mixing (e.g. (Nikurashin & Vallis, 2011), (Marshall & Speer, 2012) and (Ferrari et al., 2017)). Such a balance does not hold in ECCOv4r3, instead, the model depicts a modern global ocean in a transient state with regions of net warming (Atlantic), cooling (Indo-Pacific), and both (the deep Southern Ocean), where much of the interior up- and down-welling is not balanced by watermass transformations. In summary, we must conclude that either a) ECCOv4r3's representations of the MOC and watermass transformations are incorrect and fundamentally inconsistent (watermass transformations do not balance the inferred circulation) or b) ECCOv4r3 is correct and deep ocean density trends are indeed critical to reconcile the present-day MOC with interior watermass transformation processes, in which case equilibrium models are inadequate for the present-day MOC.

Acknowledgments

This work was supported by the National Science Foundation through award OCE-1846821. The ECCO data are publicly available at https://ecco-group.org/products.htm. The authors would like to thank Paola Cessi for providing her MATLAB scripts for ECCOv4r3 data analysis for comparison.

References

Adkins, J. (2013). The role of deep ocean circulation in setting glacial climates. *Paleoceanography*, *28*(3), 539-561. doi: 10.1002/palo.20046

Cessi, P. (2019). The Global Overturning Circulation. *Annual Review of Marine Science*, *11*(1), 249-270. doi: 10.1146/annurev-marine-010318-095241

de Lavergne, C., Madec, G., Le Sommer, J., George Nurser, A. J., & Naveira Garabato, A. C. (2016). On the consumption of Antarctic Bottom Water in the abyssal ocean. *Journal of Physical Oceanography*, 635-661. doi: 10.1175/JPO-D-14-0201.1

Desbruyères, D. G., McDonagh, E. L., King, B. A., & Thierry, V. (2017). Global and Full-Depth Ocean Temperature Trends during the Early Twenty-First Century from Argo and Repeat Hydrography. *Journal of Climate*, *30*(6), 1985-1997. doi: 10.1002/2015GL067254

ECCO Consortium, Fukumori, I., Wang, O., Fenty, I., Forget, G., Heimbach, P., & Ponte, R. (2017). ECCO Central Estimate (Version 4 Release 3). Retrieved from https://ecco.jpl.nasa.gov/drive/files/Version4/Release3/ (last accessed on 8/5/2021)

Ferrari, R., & Ferreira, D. (2011). What processes drive the ocean heat transport? *Ocean Modelling*, *38*(3-4), 171-186. doi: 10.1016/j.ocemod.2011.02.013

Ferrari, R., Jansen, M., Adkins, J., Burke, A., Stewart, A., & Thompson, A. (2014). Antarctic sea ice control on ocean circulation in present and glacial climates. *Proceedings of the National Academy of Sciences*, *111*(24), 8753-8758. doi: 10.1073/pnas.1323922111

Ferrari, R., Nadeau, L.-P., Marshall, D. P., Allison, L. C., & Johnson, H. L. (2017). A Model of the Ocean Circulation with Two Closed Basins and a Reentrant Channel. *Journal of Physical Oceanography*, *47*(12), 2887-2906. doi: 10.1175/JPO-D-16-0223.1

Forget, G., J.-M., C., Heimbach, P., Hill, C. N., Ponte, R. M., & Wunsch, C. (2015). ECCO version 4: an integrated framework for non-linear inverse modeling and global ocean state estimation. *Geoscientific Model Development*, *8*(10), 3071-3104. doi: 10.5194/gmd-8-3071-2015

Forget, G., & Ponte, R. (2015). The partition of regional sea level variability. *Progress in Oceanography*, *137*, 173-195. doi: 10.1016/j.pocean.2015.06.002

Fukumori, I., Wang, O., Fenty, I., Forget, G., Heimbach, P., & Ponte, R. (2017). Ecco version 4 release 3. Retrieved from https://www.ecco-group.org/docs/v4r3_summary.pdf doi: 1721.1/110380

Gaspar, P., Grégoris, Y., & Lefevre, J.-M. (1990). A simple eddy kinetic energy model for simulations of the oceanic vertical mixing: Tests at station Papa and long-term upper ocean study site. *Journal of Geophysical Research: Oceans*, *95*(C9), 16179-16193. doi: 10.1029/JC095iC09p16179

Gnanadesikan, A. (1999). A simple predictive model for the structure of the oceanic pycnocline. *Science*, *283*(5410), 2077-2079. doi: 10.1126/science.283.5410.2077

Gordon, A. (2001). Bottom Water Formation. *Encyclopedia of Ocean Sciences (Second Edition)*. doi: 10.1016/B978-012374473-9.00006-0

Kunze, E. (2017). The internal-wave-driven meridional overturning circulation. *Journal of Physical Oceanography*, 2673-2689. doi: 10.1175/JPO-D-16-0142.1

Lee, S.-K., Lumpkin, R., Baringer, M. O., Meinen, C. S., Goes, M., Dong, S., … Yeager, S. G. (2019). Global Meridional Overturning Circulation Inferred From a Data-Constrained Ocean and Sea-Ice Model. *Geophysical Research Letters*, *46*(3), 1521-1530. doi: 10.1029/2018GL080940

Liang, X., Wunsch, C., Heimbach, P., & Gael, F. (2015). Vertical Redistribution of Oceanic Heat Content. *Journal of Climate*, 3821-3833. doi: 10.1175/JCLI-D-14-00550.1

Lumpkin, & Speer. (2007). Global Ocean Meridional Overturning. *Journal of Physical Oceanography*, *37*(10), 2550-2562. doi: 10.1175/JPO3130.1

Marshall, J., Hill, C., & Perelman, L. (1997). Hydrostatic, quasi-hydrostatic, and nonhydrostatic ocean modeling. *Journal of Geophysical Research: Oceans*, *102*(C3), 5733-5752. doi: 10.1029/96JC02776

Marshall, J., & Speer, K. (2012). Closure of the meridional overturning circulation through Southern Ocean upwelling. *Nature Geoscience*, *5*(3), 171-181. doi: 10.1038/ngeo1391

Nadeau, L., Ferrari, R., & Jansen, M. F. (2019). Antarctic Sea Ice Control on the Depth of North Atlantic Deep Water. *Journal of Climate*, *32*(9), 2537-2551. doi: 10.1175/JCLI-D-18-0519.1

Newsom, E. R., Bitz, C. M., Bryan, F. O., Abernathey, R., & Gent, P. R. (2016). Southern Ocean Deep Circulation and Heat Uptake in a High-Resolution Climate Model. *Journal of Climate*, *29*(7), 2597-2619. doi: 10.1175/JCLI-D-15-0513.1

Nikurashin, & Vallis. (2011). A theory of deep stratification and overturning circulation in the ocean. *Journal of Physical Oceanography*, 485-502. doi: 10.1175/2010JPO4529.1

Palmer, M., Roberts, C., Balmaseda, M., Chang, Y.-S., Chepurin, G., Ferry, N., ... Xue, Y. (2015). Ocean heat content variability and change in an ensemble of ocean reanalysis. *Climate Dynamics*, *49*, 909-930. doi: 10.1007/s00382-015-2801-0

Rossby, T., Flagg, C., Chafik, L., Harden, B., & Søiland, H. (2018). A Direct Estimate of Volume, Heat, and Freshwater Exchange Across the Greenland-Iceland-Faroe-Scotland Ridge. *Journal of Geophysical Research: Oceans*, *123*(10), 7139-7153. doi: 10.1029/2018JC014250

Rousselet, L., Cessi, P., & Forget, G. (2021). Coupling of the mid-depth and abyssal components of the global overturning circulation according to a state estimate. *Science Advances*, *7*(21). doi: 10.1126/sciadv.abf5478

Russel, J., Dixon, K., Gnanadesikan, A., Stouffer, R., & Toggweiler, J. (2006). Southern Hemisphere westerlies in a warming world: Propping open the door to the deep ocean. *Journal of Climate*, 6382-6390. doi: 10.1175/JCLI3984.1

Sarmiento, L. Q. (2019). Oceanic Carbon Dioxide Uptake in a Model of Century-Scale Global Warming. *Science*, *274*(5291), 1346-1350. doi: 10.1126/science.274.5291.1346

Talley, L. (2013). Closure of the Global Overturning Circulation Through the Indian, Pacific, and Southern Oceans: Schematics and Transports. *Oceanography*, *26*(1), 80-97. doi: 10.5670/oceanog.2013.07

Tesdal, J.-E., & Haine, T. W. N. (2020). Dominant terms in the freshwater and heat budgets of the subpolar north atlantic ocean and nordic seas from 1992 to 2015. *Journal of Geophysical Research: Oceans*, *125*(10). doi: 10.1029/2020JC016435

Thompson, A., Stewart, A., & Bischoff, T. (2016). A Multibasin Residual-Mean Model for the Global Overturning Circulation. *Journal of Physical Oceanography*, *46*(9), 2583-2604. doi: 10.1175/JPO-D-15-0204.1

Toggweiler, J., Russell, J. L., & Carson, S. R. (2006). Midlatitude westerlies, atmospheric CO2, and climate change during the ice ages. *Paleooceanography*, *21*(PA2005). doi: 10.1029/2005PA001154

Walin, G. (1982). On the relation between sea-surface heat flow and thermal circulation in the ocean. *Tellus*, *34*(2), 187-195. doi: 10.1111/j.2153-3490.1982.tb01806.x

Weaver, A. J., Bitz, C. M., Fanning, A. F., & Holland, M. M. (1999). THERMOHALINE CIRCULATION: High-Latitude Phenomena and the Difference Between the Pacific and Atlantic. *Annual Review of Earth and Planetary Sciences*, *27*, 231-285. doi: 10.1146/annurev.earth.27.1.231

Wolfe, & Cessi. (2011). The Adiabatic Pole-to-Pole Overturning Circulation. *Journal of Physical Oceanography*, *41*(9), 1795-1810. doi: 10.1175/2011JPO4570.1

Wunsch, C. (2005). The total meridional heat flux and its oceanic and atmospheric partition. *Journal of Physical Oceanography*, 4374-4380. doi: 10.1175/JCLI3539.1

Wunsch, C., & Heimbach, P. (2014). Bidecadal thermal changes in the abyssal ocean. *Journal of Physical Oceanography*, 2013-2030. doi: 10.1175/JPO-D-13-096.1

Zanna, L., Khatiwala, S., Gregory, J. M., Ison, J., & Heimbach, P. (2019). Global reconstruction of historical ocean heat storage and transport. *Proceedings of the National Academy of Sciences*, *116*(4), 1126-1131. doi: 10.1073/pnas.1808838115

Zhang, R., Sutton, R., Gokhan, D., Young-Oh, K., Marsh, R., Yeager, S. G., ... Little, C. M. (2019). A Review of the Role of the Atlantic Meridional Overturning Circulation in Atlantic Multidecadal Variability and Associated Climate Impacts. *Reviews of Geophysics*, *57*(2), 316-375. doi: 10.1029/2019RG000644

Supporting Information for "The global overturning circulation and the importance of non-equilibrium effects in ECCOv4r3"

Tatsu Monkman[1] and Malte F. Jansen[1]

[1]University of Chicago

Contents of this file

1. Text S1
2. Figures S1 to S3

Introduction

The supporting information contains one text section and 3 figures supporting the results presented in our main text. Text section S1 outlines the calculations used to derive the volume budget and water-mass transformations in the surface layer. Figure S1 shows the domain masks used to define the major ocean basins in our study. Figure S2 gives a schematic representation of the various terms in the volume-budget presented in Figure 2 of the main text. Figure S3 shows the surface layer transformations in the Southern Ocean and the North Atlantic.

S1. Calculation of Surface Layer Watermass Budgets in ECCOv4r3

Ultimately, any diapycnal transport in the surface layer must be balanced by buoyancy exchange with the atmosphere and/or sea ice and mixing. We perform a volume budget decomposition within the surface layer, which is analog to the interior volume budget decomposition described in the main text. Analog to the interior volume budget discussed in the main text, we assume that the volume transport at the base of the surface layer, ψ_{surf} (minus the transport across the Greenland-Iceland-Scotland (GIS) ridge system, Ψ_{GIS}, in the case of the North Atlantic), must be balanced by heat- and freshwater-driven surface transformations, $T_{surf} = T_\Theta + T_S$, isopycnal volume change within the surface mixed layer, $\frac{d}{dt}V_{surf}$, and horizontal and vertical mixing, T_{mix}:

$$\overline{\Delta\psi(\sigma,t)} = \overline{\frac{d}{dt}V_{surf}(\sigma,t)} + \overline{T_{surf}(\sigma,t)} + \overline{T_{mix}(\sigma,t)}, \tag{1}$$

where all terms are defined as positive towards higher buoyancy (lower density). Here $\Delta\psi = \psi_{GIS} - \psi_{surf}$ in the North Atlantic and $\Delta\psi = \psi_{surf}$ in the Southern Ocean. We compute $\frac{d}{dt}V_{surf}(\sigma,t)$ as in the main text, this time including only volume changes that occur within the surface layer. We compute diapycnal transport associated with heat- and freshwater-driven surface density forcing, T_Θ and T_S, as:

$$\begin{aligned} T_\Theta(\sigma,t) &= -\frac{\partial}{\partial\sigma}\iint_{A_O(\sigma,y_1,y_2,t)} \frac{\alpha}{c_p} Q_{surf}(x,y,t)dA \\ T_S(\sigma,t) &= -\frac{\partial}{\partial\sigma}\iint_{A_O(\sigma,y_1,y_2,t)} \frac{\sigma_0}{\sigma_{fw}} \beta S_0 f_{fw}(x,y,t)dA \end{aligned} \tag{2}$$

where the integration area, $A_O(\sigma, y_1, y_2, t)$, is the outcropping region where the surface density is larger than σ within the particular basin of interest (in this case the Southern Ocean and the North Atlantic), Q_{surf} is the surface heat flux and f_{fw} is the surface freshwater flux. $\alpha = -\frac{1}{\sigma}\frac{\partial\sigma}{\partial\Theta}$ and $\beta = \frac{1}{\sigma}\frac{\partial\sigma}{\partial S}$ are the thermal expansion and haline contraction coefficients, respectively, $c_p = 3994$J/kg/K is the heat capacity of seawater,

$\sigma_0 = 1033\text{kg/m}^3$ is a reference seawater density at 2000dbar, $\sigma_{fw} = 1007\text{kg/m}^3$ is the density of freshwater at 2000dbar, and $S_0 = 35\text{g/kg}$ is a reference salinity. Here we define the heat- and freshwater-driven transformation rates, $T_\Theta(\sigma, t)$ and $T_S(\sigma, t)$, as positive for transport towards lower densities. In the North Atlantic, we calculate the rate of deep water inflow across the GIS ridge system, $\Psi_{GIS}(\sigma, t)$, by measuring the rate of meridional transport across the northern boundary of the integration area. We denote the effect of horizontal and vertical diabatic mixing within the surface layer as T_{mix}, and calculate it as the residual of the time-means of the other terms in Eq. (1).

References

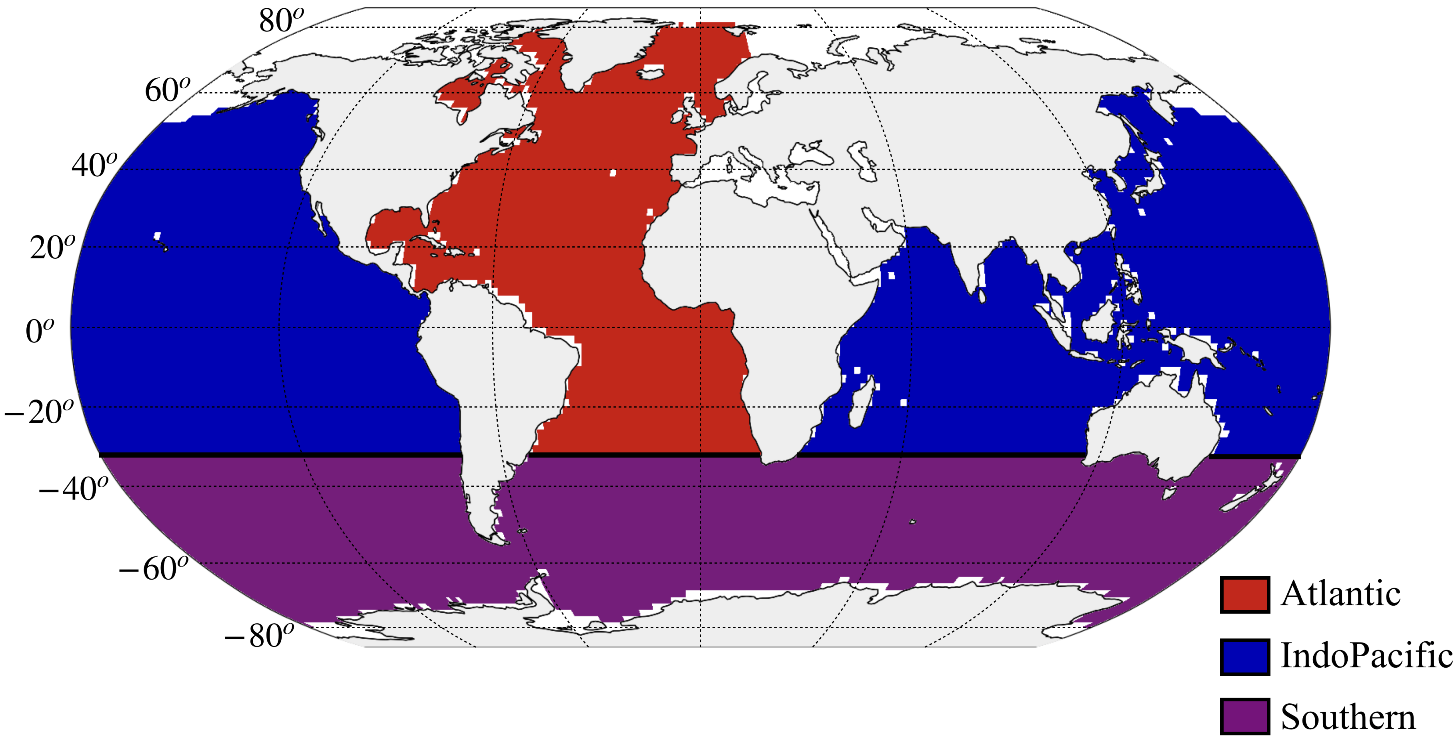

Figure S1. Basin masks used for subdividing the global ocean. The Atlantic basin (red) extends from 32^oS north into the Norwegian and Greenland seas. The Indo-Pacific basins (blue) are considered together and extend from 32^oS to the Aleutians in the North. The Southern Ocean (purple) is bounded in the north at 32^oS and extends to the coast of Antarctica.

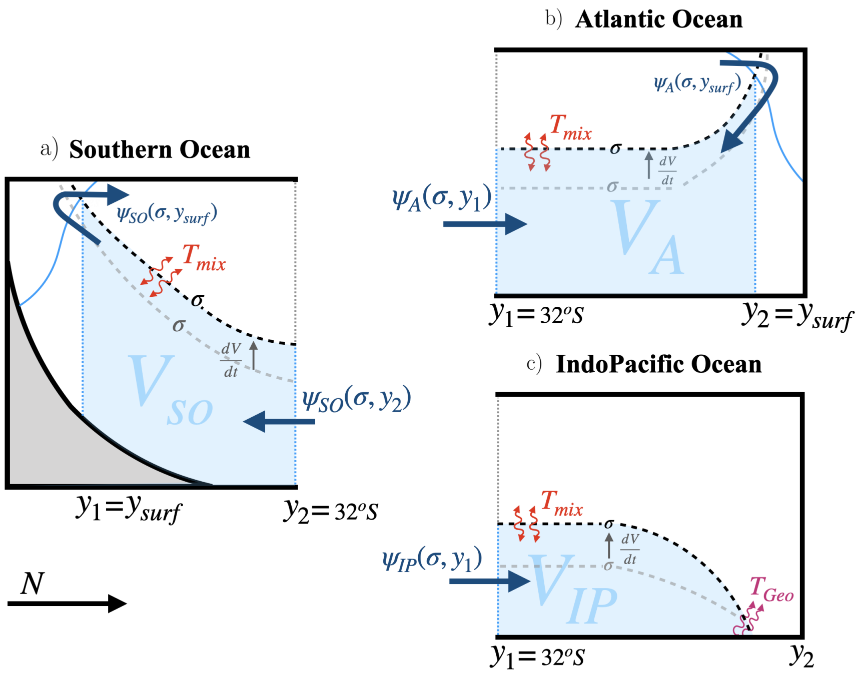

Figure S2. Schematic of the water-mass-transformation framework used in this study, applied to the Atlantic (subscript A), Indo-Pacific (subscript IP), and Southern Ocean (subscript SO). Black dashed lines indicate an isopycnal surface of density σ. Transports into and out of isopycnal volumes are indicated by arrows, with dark blue indicating advective flux ($\psi(\sigma, y)$), red diffusive flux (T_{mix}), grey apparent flux due to volume change (dV/dt), and purple transport balancing geothermal heating (T_{Geo}). Latitudes defining the southern and northern meridional bounds of the ocean basins are given by dotted blue lines and labeled y_1 and y_2, respectively, and the latitude the isopycnal intersect with the surface layer is given by y_{surf}. The bottom of the surface layer is indicated by solid blue lines.

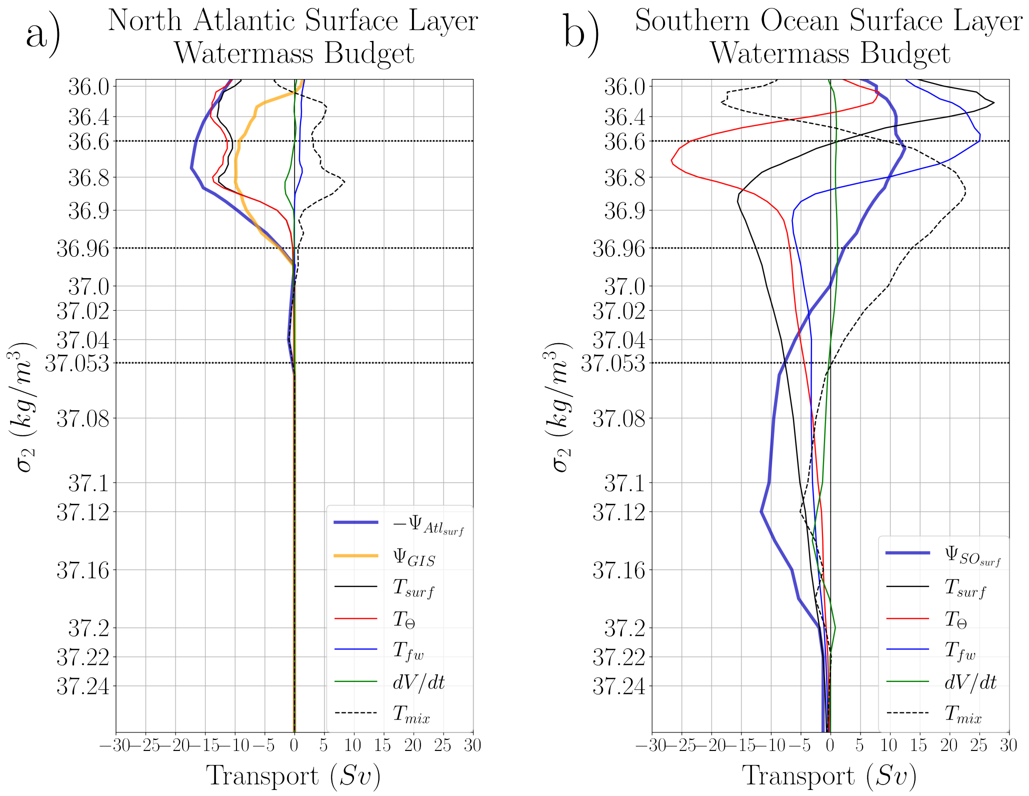

Figure S3. Water-mass-transformation decompositions in the surface layers of the North Atlantic (**a**) and Southern Ocean (**b**) high latitudes. All terms are defined positive for transformations towards higher buoyancy (lower density). Shown are the total surface transformation rate, F_{surf}, (thin, solid black) and its heat-driven, F_{Θ}, (thin, solid red) and freshwater-driven, F_{fw}, (thin, solid blue) components, as well as contributions from isopycnal volume change within the surface layer, dV/dt, (thin, solid green). Dense water inflow across the Greenland-Iceland-Scotland (GIS) ridge system, Ψ_{GIS}, is included in (**a**) (thick, solid orange). Stream function values at the bottom of the surface layer (thick, solid blue) are shown in the North Atlantic, $-\Psi_{Atl_{surf}}$, and the Southern Ocean, $\Psi_{SO_{surf}}$. Note the sign of stream function values in the North Atlantic is flipped such that negative values denote transport towards higher density. Any contributions from surface-layer mixing are calculated as a residual, T_{mix}, (dashed, black).